J Mater Sci (2021) 56:11970–11987

Metals & corrosion

Robust fluorinated siloxane copolymers via initiated chemical vapor deposition for corrosion protection

Gizem Cihanoğlu[1] and Özgenç Ebil[1,*]

[1] *Department of Chemical Engineering, Faculty of Engineering, İzmir Institute of Technology, 35430 Urla, Izmir, Turkey*

Received: 17 December 2020
Accepted: 29 March 2021
Published online: 12 April 2021

ABSTRACT

Homopolymers of 2,4,6,8-tetramethyl-2,4,6,8-tetravinylcyclotetrasiloxane (V4D4), 2-(perfluorohexyl)ethyl acrylate (PFHEA) and 2-(perfluoroalkyl)ethyl methacrylate (PFEMA) and their copolymers were synthesized via initiated chemical vapor deposition (iCVD). All coatings exhibited excellent adhesion to substrates. The corrosion resistance of iCVD coatings was investigated by electrochemical impedance spectroscopy (EIS) and potentiodynamic polarization measurements. In addition, chemical durability of various organic solvents and adhesion to the substrate were also evaluated. Tafel polarization measurements in 5 wt% NaCl solution revealed that the corrosion rates as low as 0.002 mpy on zinc substrates can be reached with 250-nm-thick iCVD-synthesized polymers which is lower than previously reported polymer coatings and more than three orders of magnitude lower than bare zinc. EIS analysis coupled with equivalent electric circuits model confirmed that poly(V4D4) and poly(PFHEA) homopolymers show extremely high protection efficiencies (~ 99%) on zinc, while poly(V4D4-co-PFHEA) copolymer with slightly lower corrosion efficiency (85–91%) provides a better anticorrosion barrier with weight loss reduction by 57 and 45% for copper and zinc, respectively, and with improved chemical and mechanical properties. The results indicate that iCVD process enables fabrication of finely tuned fluorinated siloxane copolymer conformal coatings for corrosion protection on a variety of substrates.

Introduction

A great deal of interest has arisen in polymer coatings for protection of metal surfaces against physical damage and corrosion in a wide range of applications. An ideal corrosion-resistant polymer coating should have excellent chemical stability, high mechanical strength, strong adhesion to the surface and outstanding passivation ability [1–4]. One of the advantages of using polymeric coatings is the ability to tune the morphology, chemical composition,

Handling Editor: Maude Jimenez.

Address correspondence to E-mail: ozgencebil@iyte.edu.tr

https://doi.org/10.1007/s10853-021-06060-4

adhesion and thickness of the coating to reduce the corrosion rate or minimize contact of liquid media with coated surface [5]. Although polymer coatings are physical barrier layers between the substrate and corrosive media, complete corrosion prevention is still a challenge since water, ions, and oxygen from the external environment can gradually diffuse into polymer coatings. The use of superhydrophobic polymers is among the most effective methods to inhibit direct contact of the substrate with water [4–7]. Fluorinated polymers are especially attractive as protective coatings due to their release and non-stick abilities, low abrasion and friction, low refractive index and surface energy, and antifouling properties [8–12]. The fluoropolymer matrix has a small carbon–fluorine bond polarization and provides extremely high bonding energy [13] making it a preferred candidate for applications requiring high-temperature and/or harsh-environment performance [14]. Commonly used methods to prepare fluoropolymer coatings for protection of metallic surfaces from the effects of corrosion degradation are etching [15, 16], lithography [17, 18], anodizing [15, 19], laser processing [20], coating of the surface using layer by layer deposition [21, 22], electrodeposition [23], sol–gel deposition [24, 25], and electrospinning [26, 27]. Cao et al. reported a superhydrophobic film based on polydopamine functionalized with 1H,1H,2H,2H-perfluorodecanethiol (PFDT) on a brass surface deposited using hydrothermal method to improve long-term chemical and thermal stability of films [4]. Vuoristo et al. demonstrated corrosion-resistive polyvinylidene fluoride (PVDF), ethylene chlorotrifluoroethylene (ECTFE), perfluoroalkoxy alkane (PFA) and perfluoroethylenepropylene (FEP) coatings on low alloy steel Fe 37 (St 37) by thermal spray process [28]. Combining electroetching, anodizing, sealing and surface modification methods, Mozammel and Emarati prepared a superamphiphobic surface on Al alloy 2024 (AA 2024) and demonstrated strong barrier effect of fluoropolymer coatings [15]. Xu et al. applied chronoamperometric methods to produce perfluorinated lubricant/polypyrrole composite polymer coatings for protecting low alloy steel from the corrosion [29]. The increase in the coating thickness confines the electron and heat transfer, while achieving the chemical stability for metals in electronic devices, heat conductor, and heat exchangers [30–35]. However, most of these methods still suffer from thickness nonuniformity, conformality problems due to poor surface wetting, pinhole and other defects due to fast solvent evaporation, etc. limiting their corrosion protection performance. Chemical vapor deposition (CVD) offers the smoothest conformal, cross-linked polymer coatings with good thickness control due to vapor phase polymerization process [1, 36, 37]. Recently, CVD process has been used for the fabrication of fluorinated films to improve corrosion resistance of metals in aggressive media. Ishizaki et al. [38] used microwave plasma-enhanced chemical vapor deposition (PECVD) process to fabricate superhydrophobic coatings on magnesium alloy AZ31 to improve chemical stability and corrosion resistance of AZ31 alloy. However, the corrosion rates still remain high for effective protection and fluorinated homopolymer films do not achieve chemical/mechanical robustness required in harsh environments such as strong organic solvents, acids, bases, and oxidants at varying temperature ranges [1, 39]. An ideal protective polymer coating should provide corrosion protection in such environments for months without any measurable changes in thickness, weight, composition, adhesion to substrate and its chemical and mechanical properties. A facile approach employed for the fabrication of robust polymer coatings involves cross-linking and/or establishing covalent bonding between the coating and the substrate [39–44] or using stacked polymer films [40]. Ye et al. demonstrated superhydrophobic bilayer polymer coatings with highly cross-linked polyethylene glycol diacrylate (PEGDA) bottom layer and nanostructured poly(perfluorodecyl acrylate-co-ethylene glycol diacrylate) (poly(PFDA-co-EGDA)) top layer on copper, Si wafer and polystyrene via iCVD. It was demonstrated that highly cross-linked film provided an effective oxygen barrier and good corrosion resistance [1]. Employing mechanically flexible and hydrolytically stable polysiloxane films such as poly(V4D4) in copolymer structure leads to improved chemical and mechanical properties [41–43, 45]. Lee et al. [42] fabricated a cross-linked organosilicon-acrylate copolymer thin film using V4D4 and cyclohexyl methacrylate (CHMA) via iCVD process to provide a moisture barrier with improved mechanical stability. Murthy et al. [41] used iCVD to synthesize a copolymer film with V3D3 monomer and hexavinyldisiloxane (HVDS) and reported enhanced chemical durability in both polar and nonpolar solvents. Kwak et al. fabricated a copolymer using V4D4

and perfluorodecyl methacrylate (PFDMA) via iCVD to improve the mechanical durability of fluoropolymer [45]. However, only a few studies related to iCVD-deposited poly(V4D4) films in the literature have reported their passivation performance [32]. Gleason and coworkers reported that poly(V3D3) and poly(V4D4) films exhibited excellent stability and reduced surface corrosion due to cross-linked covalent organic network [32].

Here, we report highly cross-linked, hydrophobic copolymers of V4D4 and PFHEA/PFEMA synthesized via iCVD for corrosion protection. Fabricated hydrophobic films showed excellent durability in various organic solvents and were found to be very effective for corrosion protection of metals. The low process temperature and extreme flexibility of iCVD process enable fine-tuning of physical and chemical properties of polymer films making it very attractive for the fabrication of self-cleaning, corrosion-resistant, transparent barrier layers on a large variety of substrates, including temperature-sensitive materials.

Materials and methods

Materials

Analytical-grade chemicals 2,4,6,8-tetramethyl-2,4,6,8 tetravinylcyclotetrasiloxane (V4D4, Sigma-Aldrich, 97%), 2-(perfluorohexylethyl)acrylate (PFHEA, Fluoryx Inc.) and 2-(perfluoroalkyl) ethylmethacrylate (PFEMA, Fluoryx Inc.) as monomers and tert-butyl peroxide (TBPO, Sigma-Aldrich, 98%) as initiator were used in fabrication of polymer thin films. Organic solvents such as tetrahydrofuran (THF, Panreac, 99.9%), dichloromethane (DCM, Sigma-Aldrich), *N*,*N*-dimethylformamide (DMF, Sigma-Aldrich), chloroform (Sigma-Aldrich), diethyl ether (Sigma Aldrich), 2-propanol (Sigma-Aldrich, $\geq$ 99.5%), acetone (Sigma-Aldrich, $\geq$ 99.5%), ethanol (Sigma-Aldrich, $\geq$ 99.8%), toluene (Sigma-Aldrich, $\geq$ 99.5%) and hydrogen peroxide (H_2O_2, Sigma-Aldrich) were used in durability tests. Commercially available copper and zinc plates (0.8 $\times$ 1.5 cm) were used for corrosion tests. Metal plates were polished with emery paper and then cleaned using 2-propanol (Sigma-Aldrich, $\geq$ 99.5%) before coating process.

Fabrication of polymer coatings

A custom-built iCVD system was used for the fabrication of polymer coatings. The deposition chamber was prismatic in shape with a width of 30 cm and a height of 4 cm. The top of the reactor was covered with a 2.5-cm-thick quartz plate. The reactor was equipped with a filament array suspended 2.5 cm over the substrate to supply thermal energy for the decomposition of initiator. Nichrome filaments were resistively heated via AC power supply. The substrate temperature was controlled by an external circulator (WiseCircu—refrigerated bath circulator). The reactor pressure was controlled using a throttling butterfly valve (MKS Model 253). The vacuum was provided via a rotary vane pump (BSV10, Baosi) equipped with a cold trap. Poly(V4D4), poly(PFHEA) and poly(PFEMA) homopolymers, and poly(V4D4-co-PFHEA) and poly(V4D4-co-PFEMA) copolymers were fabricated on metal and crystalline silicon (c-Si) substrates. In order to obtain sufficient vapor pressure, PFHEA and PFEMA monomers were heated to 65 and 95 °C, respectively. Monomer vapors were metered into the chamber through mass-flow controllers (MKS 1479A). For poly(V4D4) deposition, V4D4 monomer was heated to 90 °C and fed into the chamber through a special mass-flow controller (MKS 1150C). TBPO was introduced into the reactor at room temperature through a mass-flow controller (MKS 1479A). Reactor pressure was maintained at 250 mTorr throughout this study. The filament temperature was set to 250 °C for PFEMA homopolymer and fixed at 300 °C for all other homopolymer and copolymer film depositions. The average thickness of iCVD-deposited polymer films on metal substrates was 250 nm to evaluate the corrosion resistance. The deposition conditions for homopolymers and copolymers are summarized in Table 1.

Film characterization

The thicknesses of fabricated films were measured using an Mprobe-Vis20 system with a spectral range of 400–1100 nm, 2 mm spot size and 2 nm measurement accuracy. Fourier transform infrared spectroscopy (FTIR) analysis was performed using a Perkin Elmer Inc.-Spectrum BX FTIR Spectrometer for the evaluation of the quality and chemical composition of monomers and fabricated polymer films. The spectra were measured from 4000 to 650 cm^{-1}

Table 1 Process conditions for iCVD-deposited homopolymers and copolymers

Sample name	F_{V4D4}, sccm	F_{PFHEA}, sccm	F_{PFEMA}, sccm	F_{TBPO}, sccm	P_{total}, mTorr	$T_{substrate}$, °C
Poly(V4D4)	0.32	–	–	0.16	250	45
Poly(PFHEA)	–	0.39	–	0.13		25
Poly(PFEMA)	–	–	0.20	0.025		35
Poly(V4D4-co-PFHEA)	0.22	0.22	–	0.66		45
Poly(V4D4-co-PFEMA)	0.22	–	0.22	0.66		45

with a resolution of 4 cm^{-1} and accumulating over 20 scans. All spectra were baseline corrected and thickness normalized. Surface morphologies of fabricated iCVD films were investigated using scanning electron microscopy (SEM) (FEI Quanta250 system). Water contact angle (WCA) measurements were conducted to investigate the hydrophilicity of films with a Theta Optical Tensiometer.

Chemical stability and durability tests

The durability of poly(V4D4), poly(PFHEA), poly(-PFEMA) homopolymers and poly(V4D4-co-PFHEA) and poly(V4D4-co-PFEMA) copolymer films in various organic solvents was investigated following the procedures described in the literature [42]. Solubility tests were performed by immersing iCVD-coated substrates in tetrahydrofuran (THF), 2-propanol (IPA), acetone, hydrogen peroxide (H_2O_2), toluene, dichloromethane (DCM), *N*,*N*-dimethylformamide (DMF), chloroform and diethyl ether for 30 min and then drying at 70 °C for 1 h under vacuum. Adhesion to silicon wafer and metals was tested as described previously in the literature [46]. A cellophane adhesive tape was applied on the film surface and then rapidly removed from the surface at the angle that was normal to the coated surface. The percentage of delamination was calculated by dividing the test surface into equally spaced grids. The coating adhesion test was evaluated by visual inspections using a reflectometer and optical microscope.

Electrochemical characterization

Anticorrosion performance of iCVD coatings was evaluated using a Potentiostat/Galvanostat/ZRA (Gamry Model 22,162) with a tripolar electrode measurement apparatus consisting of a Pt wire as counter electrode, a saturated Ag//AgCl reference electrode and polymer film-coated Cu or Zn metal plate as working electrode. Polarization curves and electrochemical impedance spectra were obtained in 5 wt% NaCl solutions at room temperature under open-circuit conditions. Coated Cu and Zn plates were immersed in 5 wt% NaCl solution for 30 min for stabilization before the polarization measurements. Potentiodynamic polarization was performed within a potential range of open circuit potential (OCP) ± 250 mV at a scan rate of 1 mV s^{-1}. Corrosion parameters such as corrosion potential (E_{corr}), corrosion current density (I_{corr}), polarization resistance (R_p), and anodic/cathodic Tafel slopes (β_a/β_c) were calculated by using the potentiodynamic curves. For EIS analysis, AC impedance (OPC ± 5 mV) was applied between 100 MHz and 10 kHz with a sinusoidal signal perturbation of 10 mV and five points per decade.

Results and discussion

Chemical compositions of monomers, homopolymers and copolymers were investigated by FTIR analysis as shown in Fig. 1. The characteristic peaks of C=O at 1745 cm^{-1} are clearly shown in PFHEA and PFEMA spectra. The three peaks in 1140–1240 cm^{-1} region indicate stretching of $–CF_2$ and $–CF_3$ end groups. The intensity of characteristic peaks representing strong bending and stretching of C=C at 985 cm^{-1}, 995 $cm^{-1}$and 1640 cm^{-1} disappears due to complete free-radical polymerization [47–49]. For poly(V4D4) homopolymer, the peaks between 1064 cm^{-1} and 1073 cm^{-1} in FTIR spectrum represent asymmetric Si–O–Si stretching related to eight-member siloxane ring in network configuration and the peak at 1260 cm^{-1} shows the strong $Si–CH_3$ symmetric bending [41, 50, 51]. For poly(V4D4-co-PFHEA) and poly(V4D4-co-PFEMA) copolymers, the shoulders at 1140 cm^{-1} and 1240 cm^{-1} are representative of C-F chains and provide evidence of a copolymer with

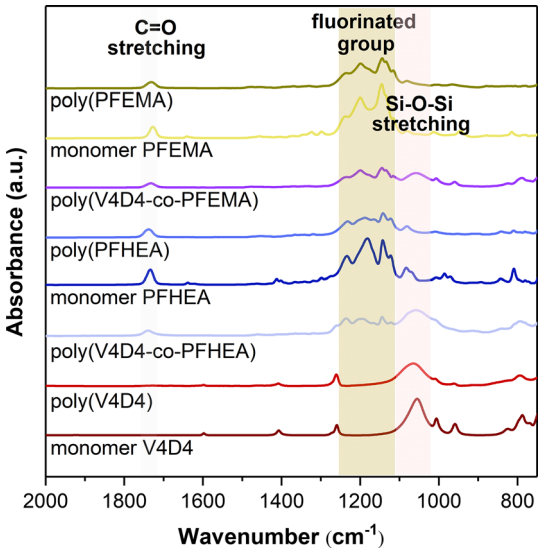

Figure 1 FTIR spectra of V4D4, PFHEA and PFEMA monomers, their homopolymers and copolymers.

cross-linked network structure. Also, the peak at 1740 cm^{-1} corresponds to stretching C=O in the acrylic group or methacrylic group [47, 49, 52]. By adjusting the flow rate of the fluorinated monomer, the composition of copolymers can be controlled. However, there may be a difference between feed composition and copolymer composition due to the monomer adsorption rate on the surface [53].

Determination of the chemical stability of iCVD films in various solvents is essential to evaluate their corrosion protection performance. The hydrolysis of the ester group is extremely slow due to the hydrophobic character of fluorinated polymers making them attractive candidates for protective coatings [43]. Most of previous studies in the literature related to hydrophobic films as protective layers have solely used WCA measurements to claim good chemical stability. Chemical stability of iCVD homopolymer films deposited on c-Si wafer was measured by the change in film thickness after immersion in various organic solvents including THF, DCM, acetone (polar aprotic solvents), IPA, ethanol, H_2O_2 (polar protic solvents), toluene, chloroform and diethyl ether (nonpolar solvents) for 30 min. Figure 2 shows relative thickness change and absolute WCA values of poly(PFHEA) and poly(PFEMA) homopolymers after immersion in solvents. Even without any cross-linking or surface grafting, both films showed good durability in organic solvents. The relative thickness change of poly(PFHEA) homopolymer films was less than 5% with the exception of diethyl ether in which a 10% thickness change was measured. On the other hand, poly(PFEMA) films performed better with less than 1.5% thickness loss except THF and diethyl ether in which 13 and 15% changes were measured, respectively. The change in WCA for homopolymer films after immersion in solvent is also shown in Fig. 2. The lowest WCA for poly(PFHEA) homopolymer was measured after immersion in diethyl ether in which the highest thickness reduction was also observed. Immersion in solvents resulted in slight reduction in WCA of poly(PFEMA) except THF and diethyl ether in which WCA changed significantly. This observation is also in line with thickness measurements shown in Fig. 2b. However, poly(-PFEMA) homopolymers still showed hydrophobicity after immersion test. The results indicate that iCVD-fluorinated homopolymer films exhibit good chemical resistance against organic solvents. FTIR spectroscopy was also used to investigate durability of poly(PFHEA) and poly(PFEMA) homopolymers films after immersion tests (see Fig. S1 and Table S2 in Supporting Information). Although peak intensities were slightly decreased, all characteristic peaks were still visible after the immersion in diethyl ether confirming durability of homopolymers in most organic solvents. In addition to simple immersion tests in various organic solvents, homopolymer films were also subjected thermal and ultrasonic treatment with mechanical mixing in DCM which is a very strong solvent. It was found that only strong ultrasonic treatment was able to effectively remove homopolymer films from the surface (see Fig. S2, Fig. S3 and Table S3 in Supporting Information).

Similar to homopolymer films, the chemical stability of poly(V4D4-co-PFHEA) and poly(V4D4-co-PFEMA) copolymers deposited on c-Si substrates was evaluated by the change in film thickness after immersion in strong organic solvents as described in the literature [42]. The relative changes in thicknesses of homopolymers and copolymer films before and after immersion in THF, DCM, DMF, chloroform and diethyl ether for 30 min are shown in Fig. 3. Overall, poly(V4D4-co-PFEMA) films exhibited better resistance against organic solvents compared to poly(V4D4-co-PFHEA) polymer films. Poly(V4D4-co-PFHEA) polymers showed up to 30% thickness loss, while the maximum thickness loss was around 15% for poly(V4D4-co-PFEMA). This might be related to the differences between the length of the pendent

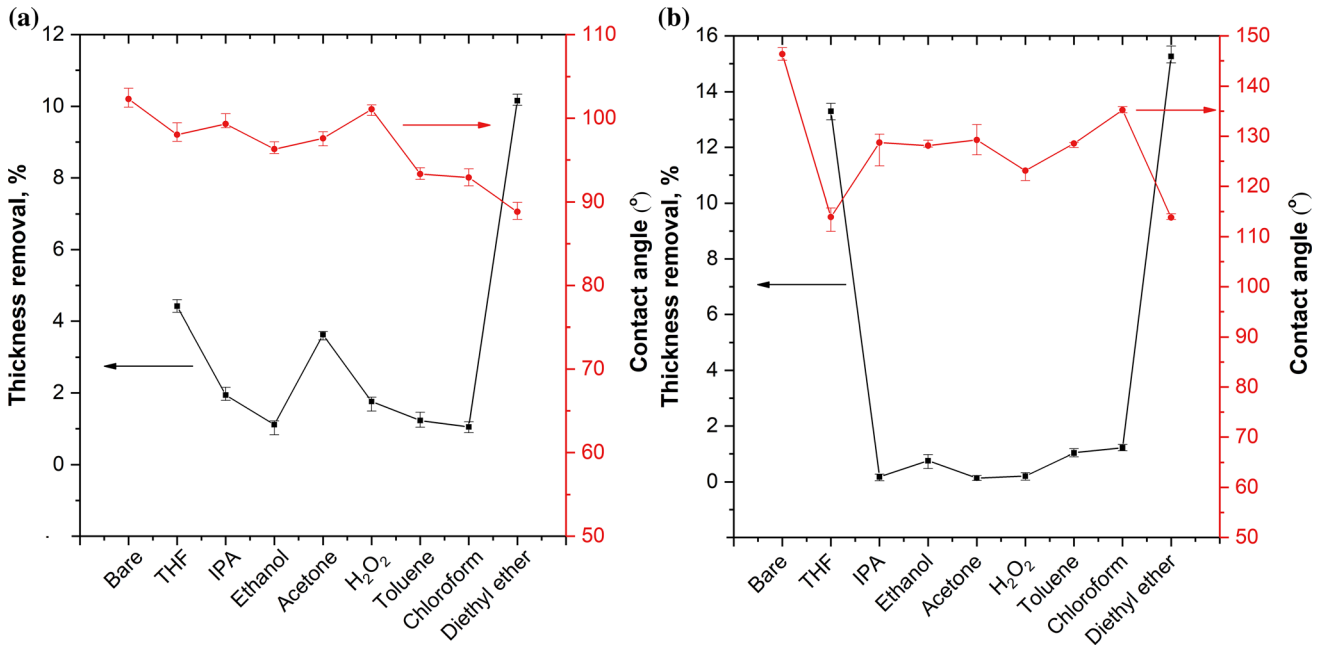

Figure 2 Relative thickness change and absolute WCA values for **a** poly(PFHEA) and **b** poly(PFEMA) homopolymer films after immersion in various solvents.

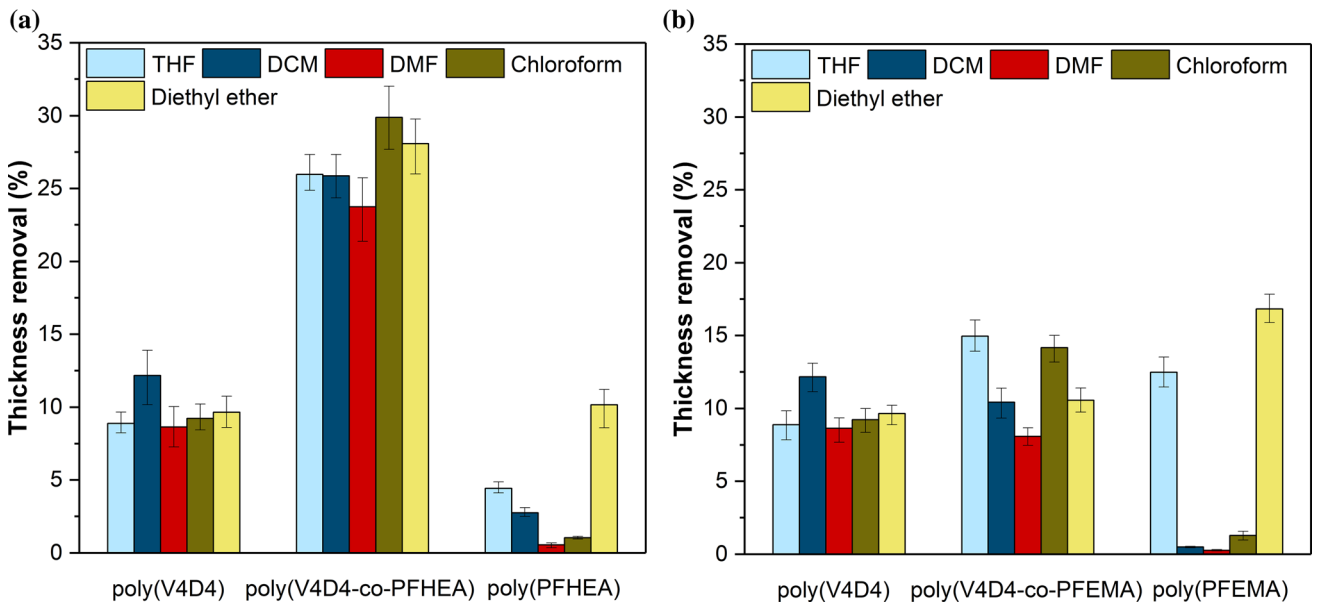

Figure 3 Relative change in film thickness for homopolymers and copolymers with **a** PFHEA and **b** PFEMA.

perfluorocarbon chains (n_{PFEMA} = 4–10; n_{PFHEA} = 6) [47, 54]. It is also possible that formation of small molecules or short side chains due to certain process conditions might lead to insufficient cross-linking of polymer making it sparingly soluble [41]. In addition to chemical composition, the durability of copolymer films in a solvent is also affected by overall quality and uniformity of the film as well as the surface properties of the substrate on which the copolymer is deposited. FTIR analysis confirmed existence of V4D4 and PFHEA/PFEMA moieties for both copolymer films after solubility test, indicating good resistance against strong solvents. SEM analysis was also performed to evaluate surface morphologies of coatings before and after immersion test. As expected, a slight change in surface morphology was observed after

immersion in solvent; however, the highest change was observed in copolymer samples after immersion in diethyl ether. This change in surface morphology and roughness might explain relatively high thickness removal for copolymers since thickness measurements may also result from the position difference (see Figs. S4 and S5 in Supporting Information).

The corrosion protection performances of homo- and copolymers on copper and zinc substrates were evaluated via Tafel polarization measurements as shown in Fig. 4. The potentiodynamic polarization was measured after achieving constant OCP. Tafel curves were generated for poly(V4D4), poly(PFHEA), poly(PFEMA) homopolymers as well as poly(V4D4-co-PFHEA) and poly(V4D4-co-PFEMA) copolymers in 5 wt% NaCl solution. The values of the anodic and cathodic Tafel slopes (β_A and β_C) provide valuable information on corrosion protection efficiency of the coatings; β_C is attributed to the hydrogen evolution in a cathodic branch, while β_A corresponds to the metal dissolution in an anodic branch [5]. The important corrosion parameters, i.e., corrosion current density (I_{corr}), corrosion potential (E_{corr}), cathodic/anodic Tafel slopes (β_c/β_a), received from Tafel curves are listed in Table 2. Experimental polarization resistance (R_p) was calculated by Stern-Geary equation [15]:

$$R_p = \frac{\beta_A \beta_C}{2.303 I_{corr}(\beta_A + \beta_C)} \quad (1)$$

where I_{corr} is the corrosion current in amps, β_A is the anodic beta Tafel coefficient for anodic portion in V dec^{-1}, β_C is the cathodic beta Tafel coefficient for anodic portion in V dec^{-1}. The lower corrosion current density and higher corrosion potential signify a lower corrosion rate which means better corrosion protection [1, 2]. Unlike wet processes, most iCVD-deposited polymers exhibit very small or no porosity due to lack of solvent in polymerization environment. Since polymerization reactions occur on cooled substrate surface and not in gas phase, iCVD coatings can conform to the overall geometry making them highly suitable to use as anticorrosion coatings. Still, the porosity of iCVD coatings on metal surfaces was calculated from potentiodynamic polarization measurements, using Eq. 2 [55]:

$$\text{Porosity} = \frac{R_{p_{bare}}}{R_{p_{coated}}} \times 10^{-\left(\frac{|\Delta E_{corr}|}{\beta_a}\right)} \quad (2)$$

where R_{pbare} is the polarization resistance of bare metal, $R_{pcoated}$ is the polarization resistance of coated metal, ΔE_{corr} is the difference between corrosion potentials, and β_a is the anodic Tafel slope for bare metal. The protection efficiency (η %) of the coatings was calculated from I_{corr} values of the samples, using the expression [29]:

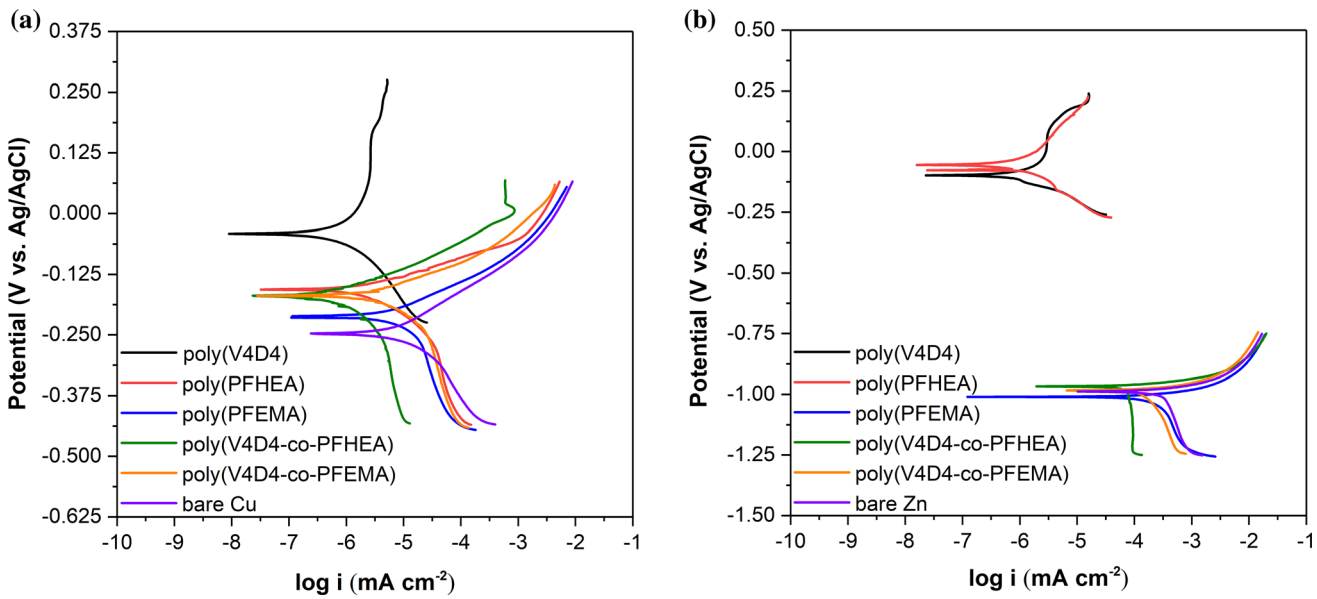

Figure 4 Potentiodynamic polarization measurements for iCVD coatings on **a** copper and **b** zinc substrates.

Table 2 Kinetic parameters of iCVD polymers on copper and zinc substrates

	E_{corr}, mV	I_{corr}, μA	β_A, mV/dec	β_C, mV/dec	Corrosion rate, mpy	R_p x 10^{-3}, kΩ/cm^2	Porosity, %	η, %
Copper								
Bare	– 247	18.9	106	159	0.182	1.46		
Poly(V4D4)	– 42	4.2	1922	213	0.046	19.82	6.33	77.78
Poly(PFHEA)	– 156	7.8	68	201	0.086	2.83	3.73	58.73
Poly(PFEMA)	– 213	14.4	87	248	0.158	1.94	1.57	23.81
Poly(V4D4-co-PFHEA)	– 169	1.7	59	249	0.018	12.18	0.65	91.01
Poly(V4D4-co-PFEMA)	– 169	12	77	245	0.132	0.25	3.75	36.51
Zinc								
Bare	– 988	939	152	10^{15}	9	8.79		
Poly(V4D4)	– 98	2	531	137	0.024	20.54	1.81	99.79
Poly(PFHEA)	– 60	0.1	136	92	0.002	100.08	0.85	99.99
Poly(PFEMA)	– 910	874	156	10^{15}	8.05	9.05	4.46×10^{-6}	6.92
Poly(V4D4-co-PFHEA)	– 967	140	87	10^{15}	1	5.69	2.92×10^{-8}	85.09
Poly(V4D4-co-PFEMA)	– 983	550	139	10^{15}	6	1.45	1.62×10^{-7}	41.43

dec decade, *mpy* mils per years

$$\eta(\%) = \frac{I_{corr_{bare}} - I_{corr_{coated}}}{I_{corr_{bare}}} \times 100 \quad (3)$$

The results suggest that siloxane films significantly increase E_{corr} and provide better corrosion protection for metal surfaces. Copolymerization of V4D4 with fluorinated monomers results in lower E_{corr} compared to poly(V4D4) homopolymer; however, chemical and mechanical stability in strong organic solvents is greatly improved. For copper substrates, poly(V4D4-co-PFHEA) coatings showed the highest protection efficiency (91%) and the lowest corrosion rate (0.018 mpy). All homopolymers exhibited lower corrosion rates and higher protection efficiencies than poly(V4D4-co-PFEMA) copolymer. On zinc substrates, poly(V4D4) and poly(PFHEA) homopolymers followed by poly(V4D4-co-PFHEA) copolymer showed lower corrosion rates and higher protection efficiencies.

EIS analysis is a powerful tool that provides valuable information about corrosion protection performance, robustness of coatings and electrochemical activity at coating/metal interface. EIS analysis was performed for bare metals and polymer-coated metals from 100 MHz to 10 kHz in 5 wt% NaCl solution. Measurements were performed after 30 min of immersion for stabilization. Nyquist plots of bare metals and polymer-coated metals (copper and zinc) are presented in Fig. 5 with insets showing enlarged Nyquist plots. The impedance plots of the copolymer coatings showed that there are two different capacitive loops. The first loop refers to the polymer coating itself, while the second one is attributed to the dissolution process taking place at the coating–metal interface [56]. The Nyquist semicircles with wider diameters indicate better corrosion resistance [2]. As shown in Fig. 5, homopolymers of poly(V4D4) and poly(PFHEA) and their copolymer poly(V4D4-co-PFHEA) coating exhibit better anticorrosion and barrier performance. The variations between poly(V4D4-co-PFHEA) and poly(V4D4-co-PFEMA) copolymer performance might be due to differences in cross-linked network due to acrylate and methacrylate groups linked to V4D4 [57].

Bode plots of samples from the same experiment are shown in Fig. 6. Bode plots reveal the circuit behavior in terms of circuit elements either as resistor (Θ = 0 degrees) or capacitor (Θ = – 90 degrees), and provide information about electrochemical activity at the coating–metal interface and the extent of water diffusion or penetration [6, 58]. The shift in time constant through high frequency to medium/low

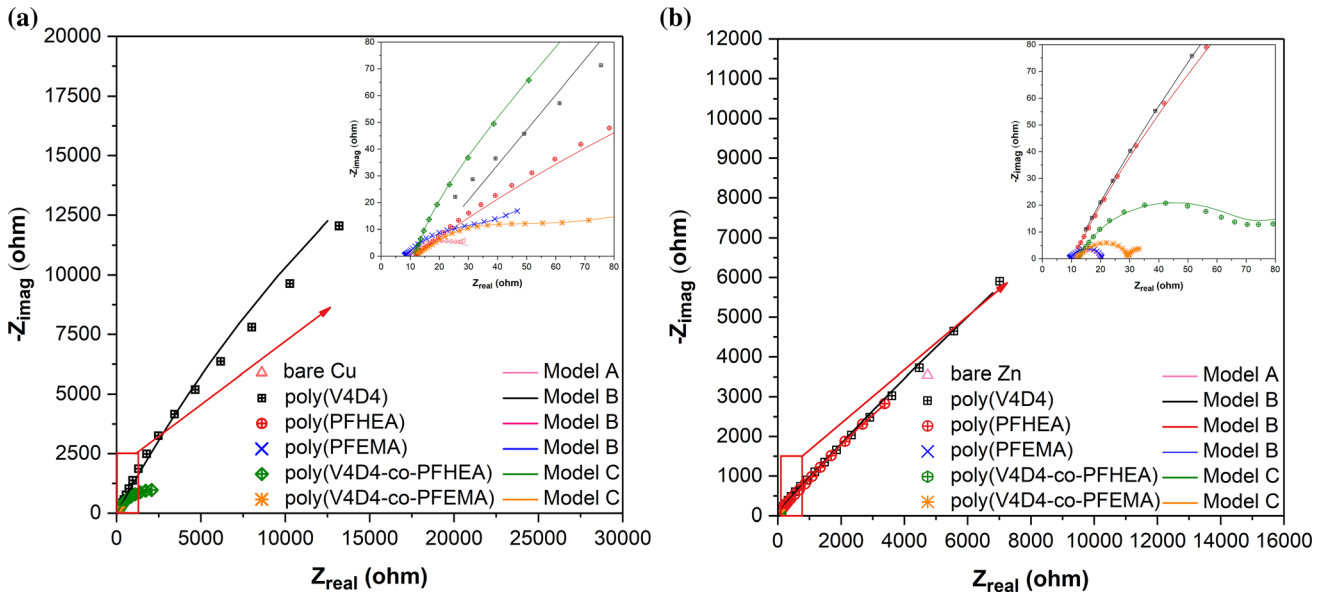

Figure 5 Nyquist plots of iCVD polymers on **a** copper and **b** zinc substrates.

frequency indicates the presence of a passivation layer on the top of metal surface [59]. The medium- to low-frequency phenomenon is associated with the acceleration of interaction between coating and metal surface [60]. Figure 6 shows circuit behavior representative of a capacitor at frequencies above 100 Hz and of a resistor at frequencies below 1 Hz with the exception of poly(V4D4) and poly(PFHEA) homopolymer. In Fig. 6a and c, bare metal- and homopolymer-coated samples have only one peak at low-frequency region, while poly(V4D4-co-PFHEA)- and poly(V4D4-co-PFEMA)-coated samples showed two time constants. The phase angle of poly(V4D4-co-PFHEA) coating on copper surface shows well-defined time constants in high frequency range indicating a better corrosion barrier. However, on zinc surface the lack of high-frequency time constants implies poor or defective copolymer coatings. This observation is also in agreement with calculated protection efficiencies listed in Table 2 where poly(V4D4) and poly(PFHEA) homopolymers exhibited better protection efficiency compared to copolymer coatings, especially on zinc. Figure 6b, d shows parallel resistor–capacitor behavior of polymer coatings by illustrating the effect of measurement frequency on current flow. The current passes through the circuit capacitors at high frequencies and passes through the circuit resistors as lower frequencies [61–63]. The lower breakpoint frequency can correspond to reduction of corrosion delamination [6]. The shift in the breakpoint frequency through high frequencies might indicate electrolyte diffusion through the coating. As the frequency decreases, the trend lines diverge, and the dissimilar resistance values of polymer coatings become apparent. A coating experiencing corrosion at the substrate requires a second parallel resistor–capacitor in series with the coating resistor as observed for both copolymer coating on zinc [61–63].

Figure 7 shows three proposed Equivalent Electric Circuits (EEC) models based on Bode plot analysis to fit impedance parameters including solution resistance (R_s), resistance of the coating (R_c) which is the function of pore dimensions, constant phase element of the coating (CPE_c) characterized by the coating thickness and dielectric constant, charge transfer resistance at polymer/metal interface (R_{ct}) and constant phase element of electrical double layer (CPE_{dl}). The constant phase element (CPE) is commonly used in electric equivalent circuit to decrease the systematical error and represents deviation from true capacitance behavior which depends on a few parameters such as coating thickness and defect structure [38]. The impedance of CPE is expressed as $Z_{CPE} = Y_o^{-1}(j\omega)^{-n}$, where Y_o represents the pseudo-capacitance ($j^2 = -1$), ω is the angular frequency ($\omega = 2\pi f$) and n indicates the exponential coefficient ranging from 0 to 1 [6]. The impedance parameters of bare metals and polymer-coated metals were modeled by the electric equivalent circuit using Gamry

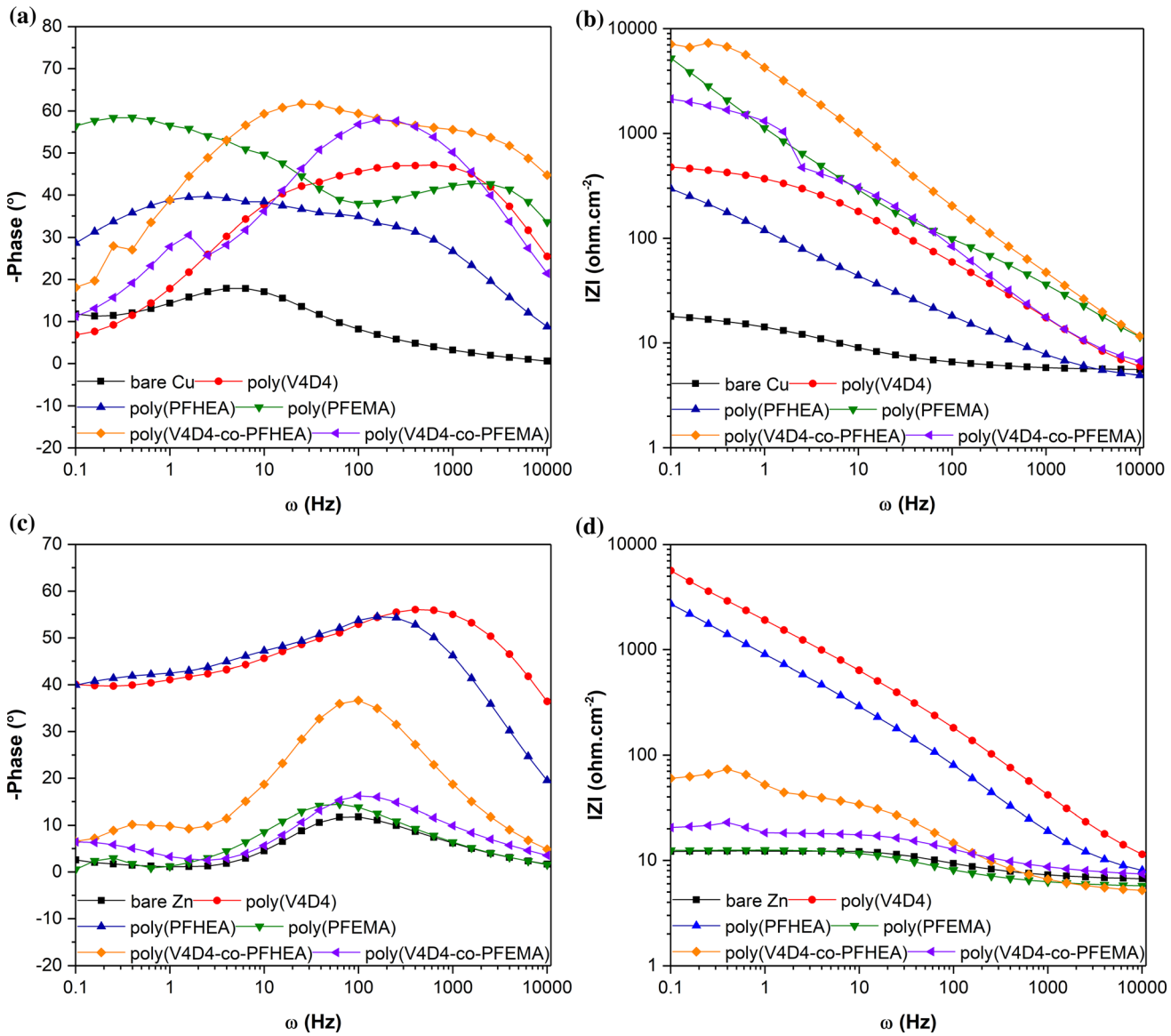

Figure 6 Bode plots of iCVD polymers on **a, b** copper and **c, d** zinc substrates.

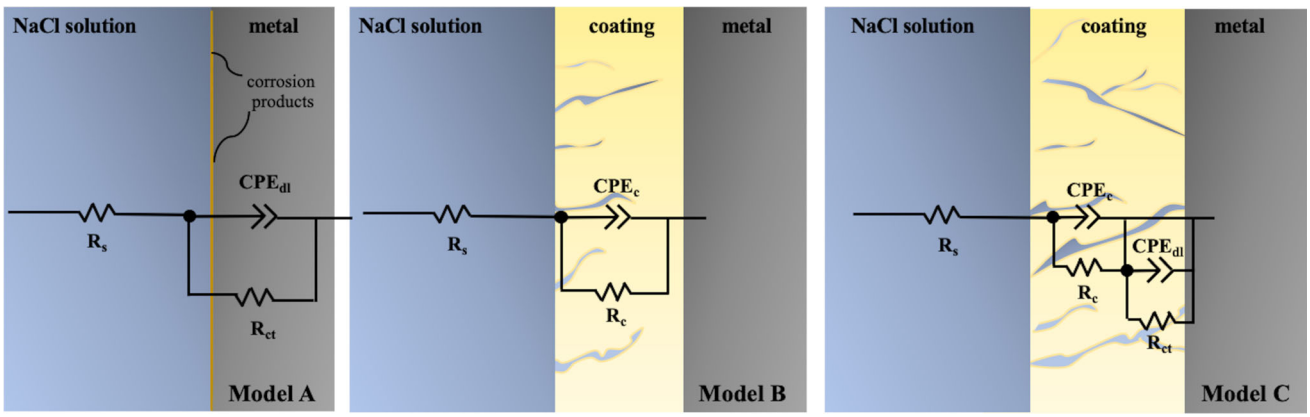

Figure 7 Equivalent electric circuits (EEC) used for fitting EIS data of bare and iCVD-coated metals.

Echem Analyst™ software. Table 3 lists model parameters of the best fit to the experimental data using EEC models shown in Fig. 7. Randles model (Model A) is one of the simplest and commonly used models describing electrochemical processes at bare metal/medium interface using solution resistance in connection with charge transfer resistance and constant phase element of electrical double layer. Model B describes corrosion process of metal surface with a polymer coating exposed to corrosive medium using solution resistance, resistance of polymer coating and constant phase element of the coating. The fit parameters, CPE_c and R_c, of Model B are used as invariable constants for the nonperfect coatings which are considered as typical for undamaged coating. Model C expands Model B with addition of charge transfer resistance at polymer/metal interface and constant phase element of electrical double layer. The higher values of R_c and R_{ct} and the lower values of CPE_c and CPE_{dl} indicate the better corrosion performance of the coating [55]. The values of electrochemical parameters from EEC fitting are in accordance with low Chi-square (χ^2) values which are similar to reported values in the literature [57, 60]. Chi-square value (χ^2) calculated between measured and model impedances should be greater than or equal to zero [64, 65]; therefore, only the best fitting models are shown in Table 3 (see Table S4 in Supporting Information for details). As shown in Table 3, poly(V4D4) homopolymer coating shows at least two orders of magnitude higher coating resistance than fluorinated homopolymers on copper. On zinc metal, poly(V4D4) and poly(PFHEA) homopolymers exhibited three orders of magnitude higher coating resistance than poly(PFEMA). In addition, poly(V4D4) and poly(PFHEA) homopolymers exhibited lower CPE_c than poly(PFEMA). The experimental data are also in good agreement with the lower values of corrosion current density (I_{corr}) or higher values of corrosion potential (E_{corr}) as shown in Table 3 [4]. For uncoated copper and zinc, R_s values describing the diffusion of ions into the solution from the oxidation of metals were determined to be 8.9 and 10.9 Ω, respectively [6, 30]. For all iCVD coatings with the exception of poly(PFEMA) homopolymer, higher R_s values were obtained. R_{ct} and CPE_{dl} parameters in Model C represents electrochemical reactions at the coating and metal interface. R_{ct} values of poly(V4D4-co-PFHEA) coatings (3.6×10^3 and 33.9 Ω for copper and zinc, respectively) suggest that these coatings effectively decrease electron-transfer activity at the coating–metal interface. A lower CPE_{dl} indicates that electrical charge distribution is minimal and the presence of corrosion products is reduced

Table 3 Electrochemical parameters extracted from the fit to the equivalent circuit models for EIS data in 5 wt% NaCl solution

Model	Uncoated Model A	Poly(V4D4) Model B	Poly(PFHEA) Model B	Poly(PFEMA) Model B	Poly(V4D4-co-PFHEA) Model C	Poly(V4D4-co-PFEMA) Model C
Copper						
R_s (Ω)	8.9	14.1	11.1	7.6	11.9	11.6
CPE_c (F m^{-1})		0.32	0.55	15.8	0.03	4.5×10^{-7}
n_1		0.58	0.42	0.47	0.84	0.46
R_c (Ω)		95.9×10^3	665.5	70.9	110.3	70.5
CPE_{dl} (F m^{-1})	7.99				0.38	13.46
n_2	0.52				0.56	1
R_{ct} (Ω)	26.13				3.6×10^3	36.7
χ^2	0.0066	0.0065	0.0015	0.0089	0.0024	0.0069
Zinc						
R_s (Ω)	10.9	12.9	12.3	9.3	12.3	11.9
CPE_c (F m^{-1})		0.17	0.37	0.42	1.1×10^{-4}	0.14
n_1		0.58	0.59	0.71	0.73	0.69
R_c (Ω)		17.4×10^3	8.8×10^3	11.4	63.4	18.5
CPE_{dl} (F m^{-1})	0.29				19.9	297.54
n_2	0.73				0.77	0.95
R_{ct} (Ω)	9.3				33.9	8.1
χ^2	0.0041	0.0014	0.0011	0.0029	0.0048	0.0029

significantly [6]. Additionally, R_c values of poly(V4D4-co-PFHEA) coatings are higher than poly(V4D4-co-PFEMA) on both copper and zinc metals.

Long-term durability and corrosion tests of copolymer coatings were performed by immersing poly(V4D4-co-PFHEA)-coated Cu and Zn plates in 5 wt% NaCl solution at room temperature for 30 days. Samples were cleaned by following the procedure described in ISO 8407 standard to remove the corrosion products [66]. Figure 8 shows the surface of uncoated and poly(V4D4-co-PFHEA)-coated copper and zinc metals immersed in 5 wt% NaCl solution for 15 and 30 days. The corrosion products increased with increasing immersion time and continuously precipitated on the surface. Uncoated copper and zinc show severe corrosion after 30 days. Despite that the copolymer film thickness was approximately 250 nm, the difference between coated and uncoated samples was visible at macroscopic scale.

In addition to visual inspection of the metal surfaces, detailed SEM analysis was also carried out to evaluate performance of iCVD coatings against corrosion. Figure 9 shows the surface morphology evolution of bare and coated metal samples exposed to 5 wt% NaCl solution after 15 and 30 days with insets showing higher magnification. The scratches on the surface of uncoated metals are due to initial rough surface cleaning using emery papers. Also, there are a few fissures and pits visible at high magnification. There is almost no difference in the surface morphology of poly(V4D4-co-PFHEA)-coated metals compared with bare metals before the corrosion test. The pitting and small pores that are uniformly distributed on the entire surface were observed after 15 days and became more pronounced after 30 days on uncoated copper. First indication of corrosion was observed on poly(V4D4-co-PFHEA)-coated copper with a small number of localized pits after 15 days. Corrosion seemed to be progressing at a much slower rate compared to uncoated sample after 30 days. During corrosion process, the electrolyte is adsorbed by the coating on copper surface [5]. The electrolyte carries water with dissolved O_2 and Cl^- and brings them in contact with bare copper surface resulting in loss of corrosion protection [55, 67]. The coating on copper surface could not provide complete corrosion protection after 30 days due to formation of copper oxides and/or chloride. The platelet-shaped microcrystals appeared on bare Zn surface after 15 days of immersion and covered the entire surface in 30 days. However, poly(V4D4-co-PFHEA)-coated Zn showed very few of these features in 30 days. After that, submicron-scale corrosion products started to appear and cover the surface. The extending exposure time to solution can result in inhibition of oxygen reduction and reduce the dissolution of zinc due to formation of passive layer as a corrosion product as reported in the literature [55, 67–69].

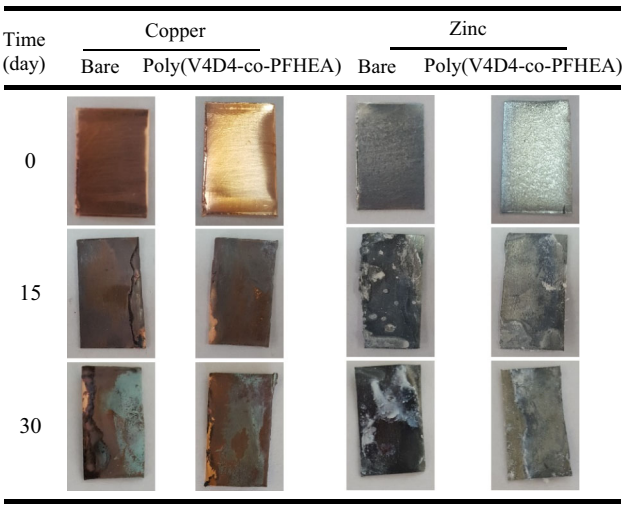

Figure 8 Coated and uncoated Cu and Zn metals after immersion in 5 wt% NaCl solution.

As listed in Table 4, measured weight losses of samples after 15 and 30 days were consistent with the potentiodynamic polarization, impedance analysis results and SEM analysis. The measured weight loss is in accordance with the release rate of M^{+2} (M: metal) on the surface of metal which leads to surface damage [5]. Poly(V4D4-co-PFHEA) coating provided a certain degree of corrosion protection as evidenced by approximately 50% less weight loss compared to uncoated samples. Surface hydrophobicity due to the presence of $-CF_3$ groups and a cross-linked structure of polymer coating seems to have decreased the formation of the corrosion products.

In addition to metals or other opaque substrates, protective coatings are also applied to optically transparent materials such as electronic and photonic devices and their components where optical transparency of the protective coating is important. It has been shown that epoxy-based iCVD copolymers exhibit excellent optical transparency in visible spectrum, good adhesion to optical glass and good mechanical strength [46]. Adhesion tests were

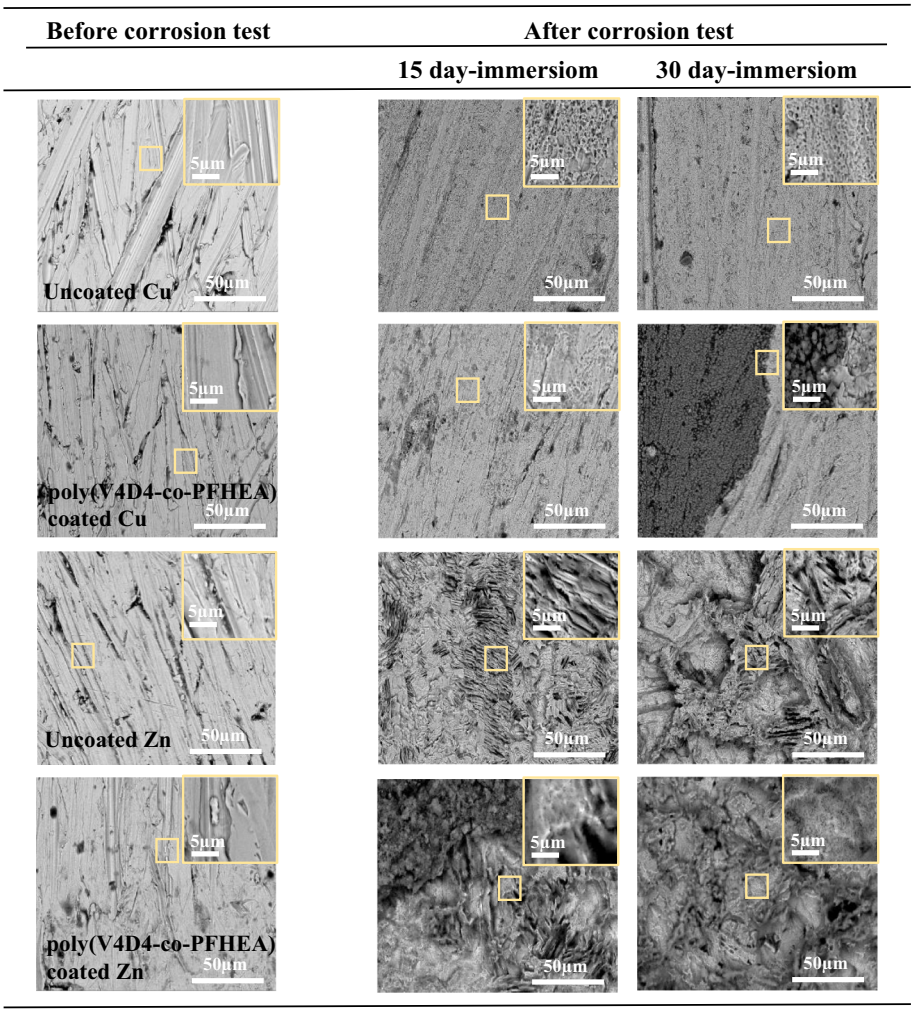

Figure 9 SEM images of uncoated and poly(V4D4-co-PFHEA) coated metals immersed in 5 wt% NaCl solution for 15 and 30 days.

Table 4 Weight losses of uncoated and coated samples after 15-day and 30-day immersion in 5 wt% NaCl

Time day	Weight loss, mg cm^{-2}			
	Cu		Zn	
	Uncoated	Poly(V4D4-co-PFHEA)	Uncoated	Poly(V4D4-co-PFHEA)
15	31.86	13.19	14.15	9.32
30	43.23	18.52	20.59	11.39

performed for poly(V4D4), poly(PFHEA), poly(-PFEMA) homopolymers and their copolymers on c-Si and metal substrates to evaluate how well iCVD polymers adhere to substrates. The optical microscope images of coatings before and after adhesion test are shown in Fig. 10. Hydrophobic materials are known to have a poor adhesion to most substrates, but they can exhibit good corrosion resistance [39, 43]. Very small pieces of fluorinated homopolymer coating (poly(PFHEA) and poly(PFEMA)) were removed by cellophane tape from the surface after the adhesion test. No other defects or delamination was observed under with optical microscope analysis of the surface after the test. The area removed during the test was less than 0.5% which still within acceptable range. Poly(V4D4) homopolymer showed excellent adhesion to the surface; no defect or delamination was observed. Similarly, poly(V4D4-co-PFHEA) and poly(V4D4-co-PFEMA) copolymers also showed excellent adhesion to substrates with no visible defects or delamination.

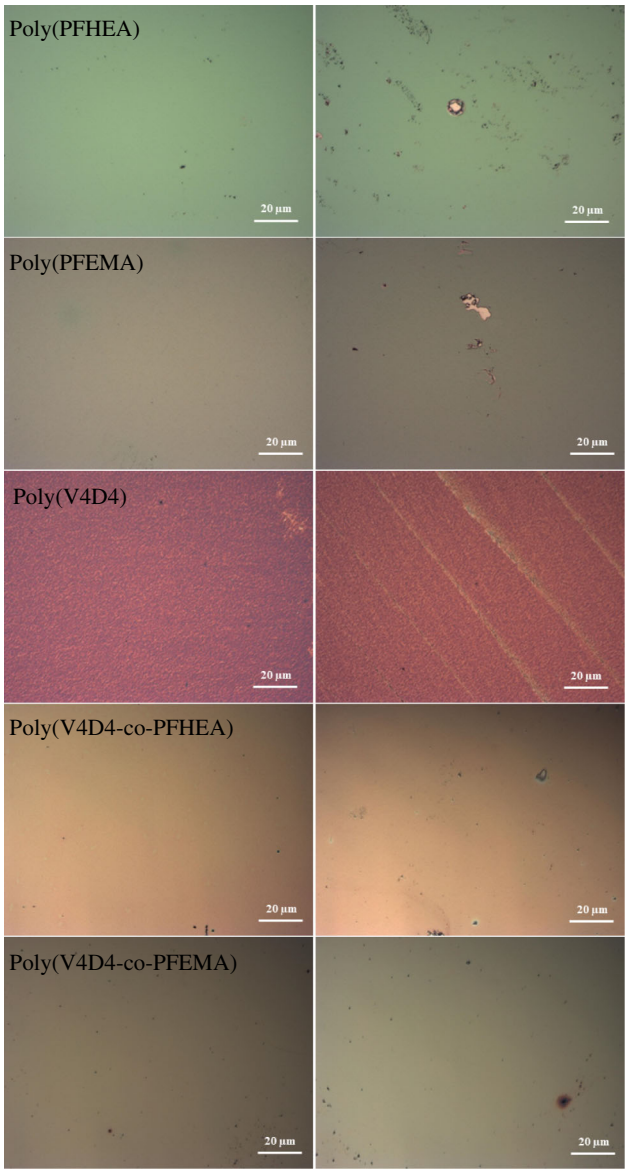

Figure 10 Optical microscopy images of polymer films before and after adhesion test.

Conclusion

Poly(V4D4), poly(PFHEA), poly(PFEMA) homopolymer, poly(V4D4-co-PFHEA) and poly(V4D4-co-PFEMA) copolymer coatings were synthesized on a variety of substrates via iCVD process. The chemical stability and durability of these polymer coatings were evaluated by adhesion to substrate tests and immersion in strong organic solvents. In addition, the corrosion protection aspects of coatings on copper and zinc substrates in 5 wt% NaCl solution were investigated by potentiodynamic polarization measurements and EIS analysis.

It was found that hydrophobic poly(PFHEA) and poly(PFEMA) homopolymers can withstand strong organic solvents well with the exception of THF and diethyl ether; however, ultrasonic treatment can remove these homopolymers from substrate surface completely. Copolymerization of PFHEA and PFEMA monomers with V4D4 was found to both increase chemical durability and improve mechanical strength of coatings since vinyl groups of V4D4 were able to bind covalently with PFHEA or PFEMA. Copolymerization also increased surface adhesion of the films. In the literature, corrosion rates for polymer coatings on copper and zinc substrates in 3.5 wt% NaCl solution were reported as 0.035–0.098 mpy and 0.063 mpy, respectively [4, 55, 69]. iCVD-synthesized polymer coatings exhibited much lower corrosion rates, as low as 0.002 mpy, in 5 wt% NaCl. Although the increase in the concentration of NaCl accelerates pitting corrosion, iCVD copolymer coatings in a higher concentration of NaCl solution still exhibit higher anticorrosion resistance than those reported in the literature [69, 70]. Between fluorinated homopolymers, poly(PFHEA) performed better than poly(-PFEMA). EIS analysis also confirmed that poly(V4D4), poly(PFHEA) and poly(V4D4-co-PFHEA) copolymer films exhibit better resistance to corrosion in 5 wt% NaCl solution. The potentiodynamic polarization measurements reveal that copolymerization of fluorinated monomers with V4D4 resulted in coatings with higher protection efficiency; 91% for poly(V4D4-co-PFHEA) and 36% for poly(V4D4-co-PFEMA), compared to homopolymer coatings; 59% for poly(PFHEA) and 24% for poly(PFEMA). Poly(V4D4-co-PFHEA) copolymer coatings showed the best anticorrosion performance with weight loss reduction by 57 and 45% for copper and zinc, respectively, and the corrosion rates by nearly a factor of 10.

The results of potentiodynamic polarization measurements and EIS analysis together with corrosion and durability indicate that poly(V4D4-co-PFHEA) copolymer coating (with 1:1 ratio of V4D4: PFHEA ratio) shows low porosity, highly hydrophobic surface, excellent adhesion, good solvent resistance and offers an effective physical and chemical protection without the need for surface pretreatment. Combining well-balanced properties of siloxane and fluorinated polymer chemistries, iCVD process is an excellent low-cost method for fabrication of

conformal protective coatings on opaque and transparent materials with different geometries.

Acknowledgements

This work was partially supported by the Scientific and Technological Research Council of Turkey (TÜBİTAK) (Grant Number 114M233).

Authors' Contributions

GC was involved in conceptualization, investigation, formal analysis, writing—original draft, visualization. ÖE contributed to writing—review and editing, supervision, project administration, funding acquisition.

Declarations

Conflict of interest The authors declare no competing financial interests.

Supplementary Information: The online version contains supplementary material available at https://doi.org/10.1007/s10853-021-06060-4.

References

[1] Chen Y, Ye YM, Chen ZR (2019) Vapor-based synthesis of bilayer anti-corrosion polymer coatings with excellent barrier property and superhydrophobicity. J Mater Sci 54:5907–5917. https://doi.org/10.1007/s10853-018-03232-7

[2] Rajitha K, Mohana KN (2020) Application of modified graphene oxide - polycaprolactone nanocomposite coating for corrosion control of mild steel in saline medium. Mater Chem Phys 241:122050. https://doi.org/10.1016/j.matchemphys.2019.122050

[3] Nautiyal A, Qiao MY, Cook JE, Zhang XY, Huang TS (2018) High performance polypyrrole coating for corrosion protection and biocidal applications. Appl Surf Sci 427:922–930. https://doi.org/10.1016/j.apsusc.2017.08.093

[4] Cao N, Miao YY, Zhang DL, Boukherroub R, Lin XG, Ju H, Li HP (2018) Preparation of mussel-inspired perfluorinated polydopamine film on brass substrates: superhydrophobic and anti-corrosion application. Prog Org Coat 125:109–118. https://doi.org/10.1016/j.porgcoat.2018.09.007

[5] Ikhe AB, Kale AB, Jeong J, Reece MJ, Choi SH, Pyo M (2016) Perfluorinated polysiloxane polysiloxane hybridized with graphene oxide for corrosion inhibition of AZ31 magnesium alloy. Corros Sci 109:238–245. https://doi.org/10.1016/j.corsci.2016.04.010

[6] Caldona EB, Smith DW, Wipf DO (2020) Protective action of semi-fluorinated perfluorocyclobutyl polymer coatings against corrosion of mild steel. J Mater Sci 55:1796–1812. https://doi.org/10.1007/s10853-019-04025-2

[7] Semiletov AM, Chirkunov AA, Kuznetsov YI (2020) Protection of aluminum alloy AD31 from corrosion by adsorption layers of trialkoxysilanes and stearic acid. Mater Corros 71:77–85. https://doi.org/10.1002/maco.201911000

[8] Chambers LD, Stokes KR, Walsh FC, Wood RJK (2006) Modern approaches to marine antifouling coatings. Surf Coat Tech 201:3642–3652. https://doi.org/10.1016/j.surfcoat.2006.08.129

[9] Graham P, Stone M, Thorpe A, Nevell TG, Tsibouklis J (2000) Fluoropolymers with very low surface energy characteristics. J Fluorine Chem 104:29–36. https://doi.org/10.1016/S0022-1139(00)00224-4

[10] Munekata S (1988) Fluoropolymers as coating material. Prog Org Coat 16:113–134. https://doi.org/10.1016/0033-0655(88)80010-4

[11] Scheirs J (1997) Modern Fluoropolymers: high performance polymers for diverse applications, 1st edn. Wiley, Chichester

[12] Yang MK, French RH, Tokarsky EW (2008) Optical properties of teflon-AF amorphous fluoropolymers. J Micro/Nanolith MEMS MOEMS 7:1–9. https://doi.org/10.1117/1.2965541

[13] Banks RE, Smart BE, Tatlow J (1994) Organofluorine chemistry: principles and commercial applications, 1st edn. Springer, US

[14] He YL, Walsh D, Shi C (2015) Fluoropolymer composite coating for condensing heat exchangers: characterization of the mechanical, tribological and thermal properties. Appl Therm Eng 91:387–398. https://doi.org/10.1016/j.applthermaleng.2015.08.035

[15] Emarati SM, Mozammel M (2020) Theoretical, fundamental and experimental study of liquid-repellency and corrosion resistance of fabricated superamphiphobic surface on Al alloy 2024. Chem Eng J 387:124046. https://doi.org/10.1016/j.cej.2020.124046

[16] Huang Y, Sarkar DK, Chen XG (2015) Superhydrophobic aluminum alloy surfaces prepared by chemical etching process and their corrosion resistance properties. Appl Surf Sci 356:1012–1024. https://doi.org/10.1016/j.apsusc.2015.08.166

[17] Jeong HE, Kwak MK, Park CI, Suh KY (2009) Wettability of nanoengineered dual-roughness surfaces fabricated by UV-assisted capillary force lithography. J Colloid Interf Sci 339:202–207. https://doi.org/10.1016/j.jcis.2009.07.020

[18] Martines E, Seunarine K, Morgan H, Gadegaard N, Wilkinson CDW, Riehle MO (2005) Superhydrophobicity and superhydrophilicity of regular nanopatterns. Nano Lett 5:2097–2103. https://doi.org/10.1021/nl051435t

[19] Nishimoto S, Sawai Y, Kameshima Y, Miyake M (2014) Underwater superoleophobicity of TiO_2 nanotube arrays. Chem Lett 43:518–520. https://doi.org/10.1246/cl.131155

[20] Steele A, Nayak BK, Davis A, Gupta MC, Loth E (2013) Linear abrasion of a titanium superhydrophobic surface prepared by ultrafast laser microtexturing. J Micromech Microeng 23:115012. https://doi.org/10.1088/0960-1317/23/11/115012

[21] Bravo J, Zhai L, Wu ZZ, Cohen RE, Rubner MF (2007) Transparent superhydrophobic films based on silica nanoparticles. Langmuir 23:7293–7298. https://doi.org/10.1021/la070159q

[22] Chunder A, Etcheverry K, Londe G, Cho HJ, Zhai L (2009) Conformal switchable superhydrophobic/hydrophilic surfaces for microscale flow control. Colloid Surf A Physicochem Eng Asp 333:187–193. https://doi.org/10.1016/j.colsurfa.2008.09.044

[23] Liu Q, Chen DX, Kang ZX (2015) One-step electrodeposition process to fabricate corrosion-resistant superhydrophobic surface on magnesium alloy. ACS Appl Mater Inter 7:1859–1867. https://doi.org/10.1021/am507586u

[24] Liang J, Hu YC, Wu YQ, Chen H (2014) Facile formation of superhydrophobic silica-based surface on aluminum substrate with tetraethylorthosilicate and vinyltriethoxysilane as co-precursor and its corrosion resistant performance in corrosive NaCl aqueous solution. Surf Coat Tech 240:145–153. https://doi.org/10.1016/j.surfcoat.2013.12.028

[25] Mahadik SA, Pedraza F, Vhatkar RS (2016) Silica based superhydrophobic coating for long-term industrial and domestic applications. J Alloy Compd 663:487–493. https://doi.org/10.1016/j.jallcom.2015.12.016

[26] Han DW, Steckl AJ (2009) Superhydrophobic and oleophobic fibers by coaxial electrospinning. Langmuir 25:9454–9462. https://doi.org/10.1021/la900660v

[27] Li XH, Ding B, Lin JY, Yu JY, Sun G (2009) Enhanced mechanical properties of superhydrophobic microfibrous polystyrene mats via polyamide 6 nanofibers. J Phys Chem C 113:20452–20457. https://doi.org/10.1021/jp9076933

[28] Leivo E, Wilenius T, Kinos T, Vuoristo P, Mantyla T (2004) Properties of thermally sprayed fluoropolymer PVDF, ECTFE, PFA and FEP coatings. Prog Org Coat 49:69–73. https://doi.org/10.1016/j.porgcoat.2003.08.011

[29] Zhu HF, Hou J, Qiu R, Zhao J, Xu JK (2014) Perfluorinated lubricant/polypyrrole composite material: Preparation and corrosion inhibition application. J Appl Polym Sci 131(1–5):40184. https://doi.org/10.1002/app.40184

[30] Liu T, Chen S, Cheng S, Tian J, Chang X, Yin Y (2007) Corrosion behavior of super-hydrophobic surface on copper in seawater. Electrochim Acta 52:8003–8007. https://doi.org/10.1016/j.electacta.2007.06.072

[31] Ates M (2016) A review on conducting polymer coatings for corrosion protection. J Adhes Sci and Technol 30:1510–1536. https://doi.org/10.1080/01694243.2016.1150662

[32] Zhao J, Wang M, Jebutu MS, Zhu M, Gleason KK (2019) Fundamental nanoscale surface strategies for robustly controlling heterogeneous nucleation of calcium carbonate. J Mater Chem A 7:17242–17277. https://doi.org/10.1039/c9ta04341a

[33] Liang T, Makita Y, Kimura S (2001) Effect of film thickness on the electrical properities of polyimide thin films. Polymer 42:4867–4872. https://doi.org/10.1016/S0032-3861(00)00881-8

[34] Kaufman FB, Schroeder AH, Engler EM, Kramer SR, Chamber JQ (1980) Ion and electron transport in stable, electroactive tetrathiafulvalene polymer coated electrodes. J Am Chem Soc 102:483–488. https://doi.org/10.1021/ja00522a007

[35] Roldughin VI, Vysotskii VV (2000) Percolation properties of metal-filled polymer films, structure and mechanisms of conductivity. Prog Org Coat 39:81–100. https://doi.org/10.1016/S0300-9440(00)00140-5

[36] Chan K, Gleason KK (2005) Initiated chemical vapor deposition of linear and cross-linked poly(2-hydroxyethyl methacrylate) for use as thin-film hydrogels. Langmuir 21:8930–8939. https://doi.org/10.1021/la051004q

[37] Coclite AM, Ozaydin-Ince G, d'Agostino R, Gleason KK (2009) Flexible cross-linked organosilicon thin films by initiated chemical vapor deposition. Macromolecules 42:8138–8145. https://doi.org/10.1021/ma901431m

[38] Ishizaki T, Hieda J, Saito N, Saito N, Takai O (2010) Corrosion resistance and chemical stability of super-hydrophobic film deposited on magnesium alloy AZ31 by microwave plasma-enhanced chemical vapor deposition. Electrochim Acta 55:7094–7101. https://doi.org/10.1016/j.electacta.2010.06.064

[39] Zhu HB, Hu WH, Zhao SP, Zhang X, Pei L, Zhao GZ, Wang Z (2020) Flexible and thermally stable superhydrophobic surface with excellent anti-corrosion behavior. J Mater Sci 55:2215–2225. https://doi.org/10.1007/s10853-019-04050-1

[40] Yoo Y, You JB, Choi W, Im SG (2013) A stacked polymer film for robust superhydrophobic fabrics. Polym Chem 4:1664–1671. https://doi.org/10.1039/c2py20963b

[41] Achyuta AKH, White AJ, Lewis HGP, Murthy SK (2009) Incorporation of linear spacer molecules in vapor-deposited

silicone polymer thin films. Macromolecules 42:1970–1978. https://doi.org/10.1021/ma802330s

[42] Seok JH, Kim SH, Cho SM, Yi GR, Lee JY (2018) Cross-linked organosilicon-acrylate copolymer moisture barrier thin film fabricated by initiated chemical vapor deposition (iCVD). Macromol Res 26:1257–1264. https://doi.org/10.1007/s13233-019-6149-2

[43] Grignard B, Vaillant A, Coninck J, Piens M, Jonas AM, Detrembleur C, Jerome C (2011) Electrospinning of a functional perfluorinated block copolymer as a powerful route for imparting superhydrophobicity and corrosion resistance to aluminum substrates. Langmuir 27:335–342. https://doi.org/10.1021/la102808w

[44] Goksel Y, Akdogan Y (2019) Increasing spontaneous wet adhesion of DOPA with gelation characterized by EPR spectroscopy. Mater Chem Phys 228:124–130. https://doi.org/10.1016/j.matchemphys.2019.02.054

[45] Lee HS, Kim H, Jeong HL, Kwak JB (2019) Fabrication of a conjugated fluoropolymer film using one-step iCVD process and its mechanical durability. Coatings 9(1–9):430. https://doi.org/10.3390/coatings9070430

[46] Ozpirin M, Ebil O (2018) Transparent block copolymer thin films for protection of optical elements via chemical vapor deposition. Thin Solid Films 660:391–398. https://doi.org/10.1016/j.tsf.2018.06.044

[47] Wang QY, Zhang QH, Zhan XL, Chen FQ (2010) Structure and surface properties of polyacrylates with short fluorocarbon side chain: Role of the main chain and spacer group. J Polym Sci A Polym Chem 48:2584–2593. https://doi.org/10.1002/pola.24038

[48] Zhang QH, Wang QY, Zhan XL, Chen FQ (2014) Synthesis and performance of novel fluorinated acrylate polymers: preparation and reactivity of short perfluoroalkyl group containing monomers. Ind Eng Chem Res 53:8026–8034. https://doi.org/10.1021/ie404217d

[49] Yin X, Song YZ, Liang ZY, Zhang B, Fang LF, Zhu LP, Zhu BK (2017) Synthesis of sulfonyl fluorinated macro emulsifier for low surface energy emulsion polymerization application. J Appl Polym Sci 134:1–9. https://doi.org/10.1002/app.44921

[50] Trujillo NJ, Baxamusa SH, Gleason KK (2009) Grafted functional polymer nanostructures patterned bottom-up by colloidal lithography and initiated Chemical Vapor Deposition (iCVD). Chem Mater 21:742–750. https://doi.org/10.1021/cm803008r

[51] O'Shaughnessy WS, Gao ML, Gleason KK (2006) Initiated chemical vapor deposition of trivinyltrimethylcyclotrisiloxane for biomaterial coatings. Langmuir 22:7021–7026. https://doi.org/10.1021/la607858

[52] Altındag IA, Akdogan Y (2021) Spectrophotometric characterization of plasticizer migration in poly(vinyl chloride) based artificial leather. Mater Chem Phys 258(1–7):123954. https://doi.org/10.1016/j.matchemphys.2020.123954

[53] Gleason KK (2012) CVD Polymers: fabrication of organic surfaces and devices, 2nd edn. Wiley-VCH, Germany

[54] Tsibouklis J, Graham P, Eaton PJ, Smith JR, Nevell TG, Smart JD, Ewen RJ (2000) Poly(perfluoroalkyl methacrylate) film structures: Surface organization phenomena, surface energy determinations, and force of adhesion measurements. Macromolecules 33:8460–8465. https://doi.org/10.1021/ma0008185

[55] Pawar P, Gaikwad AB, Patil PP (2007) Corrosion protection aspects of electrochemically synthesized poly(o-anisidine-co-o-toluidine) coatings on copper. Electrochim Acta 52:5958–5967. https://doi.org/10.1016/j.electacta.2007.03.043

[56] Sadagopan S, Muthukrishnan S, Venkatachari G, Trivedi DC (2005) Corrosion protection of steel by polyaniline (PANI) pigmented paint coating. Prog Org Coat 53:297–301. https://doi.org/10.1016/j.porgcoat.2005.03.007

[57] Sakai RT, da Cruz DL, FM, Meloc HG, Benedetti AV, Santilli CV, Suegama PH, (2012) Electrochemical study of TEOS, TEOS/MPTS, MPTS/MMA and TEOS/MPTS/MMA films on tin coated steel in 3.5% NaCl solution. Prog Org Coat 74:288–301. https://doi.org/10.1016/j.porgcoat.2012.01.001

[58] Kunst SR, Cardoso HRP, Oliveira CT, Santana JA, Sarmento VHV, Muller IL, Malfatti CF (2014) Corrosion resistance of siloxane–poly(methyl methacrylate) hybrid films modified with acetic acid on tin plate substrates: Influence of tetraethoxysilane addition. Appl Surf Sci 298:1–11. https://doi.org/10.1016/j.apsusc.2013.09.182

[59] Hsu CH, Mansfeld F (2001) Technical note: Concerning the conversion of the constant phase element parameter Y_o into a capacitance. Corrosion-Houston Tx 57:747–748. https://doi.org/10.5006/1.3280607

[60] Jüttner K (1990) Electrochemical impedance spectroscopy (EIS) of corrosion processes on inhomogeneous surfaces. Electrochim Acta 35:1501–1508. https://doi.org/10.1016/0013-4686(90)80004-8

[61] Loveday D, Peterson P, Rodgers B (2004) Evaluation of organic coatings with electrochemical impedance spectroscopy part 1: Fundamentals of electrochemical impedance spectroscopy. JCT Coatings Tech 1:46–52

[62] Loveday D, Peterson P, Rodgers B (2004) Evaluation of organic coatings with electrochemical impedance spectroscopy part 2: Application of EIS to coatings. JCT Coatings Tech 1:88–93

[63] Loveday D, Peterson P, Rodgers B (2005) Evaluation of organic coatings with electrochemical impedance spectroscopy part 3: Protocols for testing coatings with EIS. JCT Coat Tech 2:22–27

[64] Pan J, Thierry D, Leygraf C (1996) Electrochemical impedance spectroscopy study of the passive oxide film on titanium for implant application. Electrochim Acta 41:1143–1153. https://doi.org/10.1016/0013-4686(95)00465-3

[65] Feliu SJ (2020) Electrochemical impedance spectroscopy for the measurement of the corrosion rate of magnesium alloys: Brief review and challenges. Metals 10(1–22):775. https://doi.org/10.3390/met10060775

[66] ISO 8407:2009 (2009) Corrosion of metals and alloys-removal of corrosion products from corrosion test specimens.

[67] Çakmakcı I, Duran B, Duran M, Bereket G (2013) Experimental and theoretical studies on protective properties of poly(pyrrole-co-N-methyl pyrrole) coatings on copper in chloride media. Corros Sci 69:252–261

[68] Redondo MI, Sánchez de la Blanca E, García MV, González-Tejera MJ (2009) Poly(N-methyl pyrrole) electrodeposited on copper: Corrosion protection properties. Prog Org Coat 65:386–391. https://doi.org/10.1016/j.porgcoat.2009.03.003

[69] Meng Y, Liu L, Zhang D, Dong C, Yan Y, Volinsky AA, Wang LN (2019) Initial formation of corrosion products on pure zinc in saline solution. Bioact Mater 4:87–96. https://doi.org/10.1016/j.bioactmat.2018.08.003

[70] Han G, Jiang P, Wang J, Yan F (2016) Effect of NaCl concentration on wear-corrosion beviour of SAF 2507 super duplex stainless steel. RCS Adv 6:111261–111268. https://doi.org/10.1039/c6ra23030j